PHYSICAL REVIEW B **77**, 201301(R) (2008)

Phase-coherent transport in InN nanowires of various sizes

Ch. Blömers,[1] Th. Schäpers,[2,*] T. Richter,[1] R. Calarco,[1] H. Lüth,[1] and M. Marso[1]

[1]*Institute of Bio- and Nanosystems (IBN-1) and JARA Jülich-Aachen Research Alliance, Research Centre Jülich GmbH, 52425 Jülich, Germany*

[2]*Institute of Bio- and Nanosystems (IBN-1), JARA Jülich-Aachen Research Alliance, and Virtual Institute of Spinelectronics (VISel), Research Centre Jülich GmbH, 52425 Jülich, Germany*

(Received 27 February 2008; revised manuscript received 5 April 2008; published 6 May 2008)

We investigate phase-coherent transport in InN nanowires of various diameters and lengths. The nanowires were grown by means of plasma-assisted molecular beam epitaxy. Information on the phase-coherent transport is gained by analyzing the characteristic fluctuation pattern in the magnetoconductance. For a magnetic field oriented parallel to the wire axis, we found that the correlation field mainly depends on the wire cross section, while the fluctuation amplitude is governed by the wire length. In contrast, if the magnetic field is perpendicularly oriented, for wires longer than approximately 200 nm, the correlation field is limited by the phase coherence length. Further insight into the orientation dependence of the correlation field is gained by measuring the conductance fluctuations at various tilt angles of the magnetic field.

DOI: 10.1103/PhysRevB.77.201301 PACS number(s): 73.63.Nm, 73.23.−b

Semiconductor nanowires fabricated by a bottom-up approach[1–3] have emerged as very interesting systems not only for the design of future nanoscale device structures[4–6] but also to address fundamental questions connected to strongly confined systems. Regarding the latter, quantum dot structures,[7–9] single electron pumps,[10] or superconducting interference devices[11] have been realized. Many of the structures cited above were fabricated by employing III-V semiconductors, e.g., InAs or InP.[1] Apart from these more established materials, InN is particularly interesting for nanowire growth because of its low energy band gap and its high surface conductivity.[12–14]

At low temperatures, the transport properties of nanostructures are affected by the electron interference effects, i.e., weak localization, the Aharonov-Bohm effect, or universal conductance fluctuations.[15,16] The relevant length parameter in this transport regime is the phase coherence length l_ϕ, i.e., the length over which phase-coherent transport is maintained. In order to obtain information on l_ϕ, the analysis of conductance fluctuations is a very powerful method.[17–23] In fact, in InAs nanowires, pronounced fluctuations in the conductance have been recently observed and analyzed.[24]

Here, we report on a detailed study of the conductance fluctuations δG measured in InN nanowires of various sizes. Information on the phase-coherent transport is gained by analyzing the average fluctuation amplitude and the correlation field B_c. Special attention is drawn to the magnetic field orientation with respect to the wire axis, since this allowed us to change the relevant probe area for the detection of phase-coherent transport.

The InN nanowires investigated here were grown without catalyst on a Si (111) substrate by plasma-assisted molecular beam epitaxy.[14,25] The measured wires had a diameter d ranging from 42 to 130 nm. The typical wire length was 1 μm. From photoluminescence measurements, an overall electron concentration of about 5×10^{18} cm^{-3} was determined.[25]

For the samples used in the transport measurements, first, contact pads and adjustment markers were defined on a SiO_2-covered Si (100) wafer. Subsequently, the InN nanowires were placed on the patterned substrate and individually contacted by the Ti/Au electrodes. Since the typical contact resistance per contact was relatively low, $(165\pm25)\Omega$, the contact separation was taken as the effective length L. The contact resistance was determined by measuring wires with different contact separations. Four wires labeled as A, B, C, and D will be discussed in detail below. Their parameters are summarized in Table I. In order to improve the statistics, additional wires that are not specifically labeled were included in part of the following analysis. A micrograph of a typical contacted wire is depicted in Fig. 4 (inset).

The transport measurements were performed in a magnetic field range from 0 to 10 T at a temperature of 0.6 K. In order to vary the angle between the wire axis and the magnetic field B, the samples were mounted in a rotating sample holder. The rotation axis was perpendicularly oriented to the magnetic field and to the wire axis. The magnetoresistance was measured by using a lock-in technique with an ac bias current of 30 nA.

The fluctuation pattern for nanowires with different dimensions is depicted in Fig. 1(a). Here, the normalized conductance fluctuations δG for wires A–C, which are comprised of successively increasing diameters, are plotted as a function of the magnetic field B. The field was oriented parallel to the wire axis. The measurements were performed up to a relatively large field of 10 T. This is justified since even

TABLE I. Dimensions and characteristic parameters of the different wires: length L, wire diameter d, root mean square of the conductance fluctuations rms(G), and correlation field B_c. The latter two parameters were determined for B parallel to the wire axis.

Wire	L (nm)	d (nm)	rms(G) (e^2/h)	B_c (T)
A	205	58	1.35	0.38
B	580	66	0.58	0.22
C	640	75	0.52	0.21
D	530	130	0.81	0.15

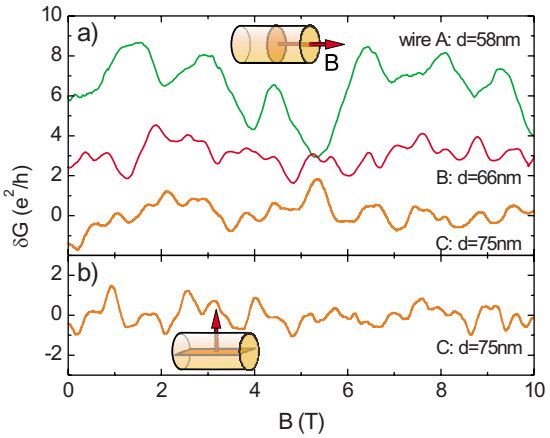

FIG. 1. (Color online) (a) Conductance fluctuations normalized to e^2/h for wires with different lengths and diameters. The curves are offset for clarity. As illustrated by the sketch, the magnetic field is axially oriented. (b) Conductance fluctuations of wire C with a magnetic field perpendicularly oriented to the wire axis.

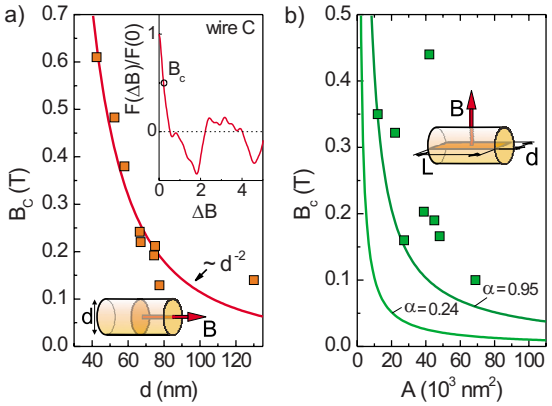

FIG. 2. (Color online) (a) Correlation field B_c as a function of the wire diameter d. As illustrated in the schematics, the magnetic field B was axially oriented. The solid lines correspond to the calculated correlation field. The inset shows $F(\Delta B)/F(0)$ for wire C. (b) B_c as a function of the maximum area $A=Ld$ (see schematics) of the wire. The magnetic field is oriented perpendicular to the wire axis. The solid lines represent the calculated lower boundary correlation fields assuming $\alpha=0.95$ and 0.24, respectively.

at 10 T the estimated cyclotron diameter of 70 nm just begins to become comparable to the wire diameter. The conductance variations were determined by first subtracting the typical contact resistance and then by converting the resistance variations to conductance variations. It can clearly be seen in Fig. 1(a) that for the narrowest and shortest wire, i.e., wire A, the conductance fluctuates with a considerably larger amplitude than for the other two wires with larger diameters and lengths. The parameter quantifying this feature is the root mean square of the fluctuation amplitude rms(G) defined by $\sqrt{\langle \delta G^2 \rangle}$. Here, $\langle \cdots \rangle$ represents the average over the magnetic field. For quasi-one-dimensional systems, where phase coherence is maintained over the complete wire length, it is expected that rms(G) is in the order of e^2/h.[19–21] As one can infer from Table I, for the shortest nanowire, i.e., wire A, rms(G) falls within this limit. For the other two wires, the rms(G) values are smaller than e^2/h (cf. Table I). Thus, for these wires, it can be concluded that the phase coherence length l_ϕ is smaller than the wire length L.

Beside rms(G), another important parameter is the correlation field B_c, quantifying on which field scale the conductance fluctuations take place. The correlation field is extracted from the autocorrelation function of δG defined by $F(\Delta B)=\langle \delta G(B+\Delta B)\delta G(B)\rangle$.[21] The magnetic field corresponding to half maximum of the autocorrelation function $F(B_c)=\frac{1}{2}F(0)$ defines B_c. The B_c values of the measurements shown in Fig. 1 are listed in Table I. Obviously, for wire A, which has the smallest diameter, one finds the largest value of B_c. In a semiclassical approach, it is expected that B_c is inversely proportional to the maximum area A_ϕ perpendicular to B, which is enclosed phase coherently,[19,21,23]

$$B_c = \alpha \frac{\Phi_0}{A_\phi}. \tag{1}$$

Here, α is a constant in the order of 1 and $\Phi_0=h/e$ is the magnetic flux quantum. As long as phase coherence is maintained along the complete circumference, A_ϕ is equal to the wire cross section $\pi d^2/4$ and thus one expects $B_c \propto 1/d^2$. The B_c values given in Table I follow this trend, i.e., becoming smaller for increasing diameter d. As can be recognized in Fig. 2 (inset), $F(\Delta B)$ also shows negative values at larger ΔB. This behavior can be attributed to the limited number of modes in the wires, as was previously observed for small size semiconductor structures.[26,27] However, as discussed by Jalabert *et al.*,[26] at small fields $F(\Delta B)$ and thus B_c being calculated fully quantum mechanically correspond well to the semiclassical approximation.

In order to elucidate the dependence of B_c on the wire diameter in more detail, a larger number of wires were measured. As can be seen in Fig. 2(a), B_c systematically decreases with d. Leaving out wire D, which has the largest diameter, the decrease in B_c is well described by a $1/d^2$ dependence. As mentioned above, for short wires ($L \approx 200$ nm), we found that phase coherence is maintained over the complete length. This length corresponds to a circumference of a wire with a diameter of about 64 nm. Except for wire D, d is in the order of that value, so that one can expect that phase coherence is maintained within the complete cross section. For the parameter α, we found a value of 0.24, which is a factor of 4 smaller than the theoretically expected value of 0.95.[23] Choosing $\alpha=0.95$ would result in lower bound values of B_c being larger than all corresponding experimental values, which is physically unreasonable. We attribute the discrepancy to the different geometrical situation, i.e., for the latter, a confined two-dimensional electron gas with a perpendicularly oriented magnetic field was considered.[23] In our case, the field is oriented parallel to the wire axis, thus the closed electron trajectories can also be extended along the magnetic field axis. This difference probably modifies the ensemble of trajectories being relevant for α. In addition, an inhomogeneous carrier distribution within the cross section, i.e., due to a carrier accumulation at the surface,[28] can also result in a disagreement between experiment and theoretical models. As can be seen in Fig. 2(a), the

data point of the wire with the largest diameter of 130 nm, i.e., wire D, is found above the calculated curve. This indicates that for this sample, A_ϕ is smaller than the wire cross section, i.e., l_ϕ is smaller than the circumference. The latter statement is supported by previous measurements of l_ϕ on InN nanowires.[29] Thus, the wire with the largest diameter cannot be considered as purely one dimensional.

Next, we will focus on measurements of δG with a magnetic field oriented perpendicular to the wire axis. As a typical example, δG of wire C is shown in Fig. 1(b). Here, a correlation field of 0.17 T was extracted, which is smaller than the value of corresponding measurements with B parallel to the wire axis [cf. Fig. 1(a) and Table I]. The smaller value of B_c can be attributed to the effect that now the relevant area for magnetic flux-induced interference effects is no longer limited by the relatively small circular cross section but rather by a larger area within the rectangle defined by L and d, as illustrated by the schematics in Fig. 2(b).

In Fig. 2(b), the B_c values of various wires are plotted as a function of the maximum area $A_{max}=Ld$ penetrated by the magnetic field. As a reference, the calculated curve using Eq. (1) and assuming $A_\phi=A_{max}$ are also plotted. It can be seen that the B_c values of two wires with small areas, including wire A, match to the theoretically expected ones if one takes $\alpha=0.95$, as given by Beenakker and van Houten.[23] This corresponds to the case of phase-coherent transport across the complete wire, as was, in the case of wire A, already concluded from the rms(G) analysis. For all other wires, the B_c values are above the theoretically expected curve, which correspond to the case $A_\phi<A_{max}$. At this point, one might argue that for B oriented along the wire axis, a better agreement is found for $\alpha=0.24$. However, as can be seen in Fig. 2(b), if one assumes $\alpha=0.24$, all experimental values are above the calculated curve, i.e., $A_\phi<A_{max}$. This does not agree with the observation that for short wires, rms(G) is in the order of e^2/h. We attribute the difference between the appropriate α values for different field orientations to the different characters of the relevant area penetrated by the magnetic flux, e.g., due to carrier accumulation at the surface.

Beside B_c, we also analyzed the fluctuation amplitude for five different wires with B oriented perpendicular to the wire axis. Here, only wires with comparable diameters of 75 ± 5 nm were chosen. It can be seen in Fig. 3 that rms(G) tends to decrease with increasing wire length L. From the previous discussion of B_c, it was concluded that for long wires, as is the case here, $l_\phi<L$. In this regime, rms(G) is expected to depend on L as[21,23]

$$\mathrm{rms}(G)=\beta\frac{e^2}{h}\left(\frac{l_\phi}{L}\right)^{3/2}, \tag{2}$$

with β in the order of 1. The above expression is valid as long as the thermal diffusion length $l_T=\sqrt{\hbar\mathcal{D}/k_BT}$ is larger than l_ϕ. Here, $\mathcal{D}$ is the diffusion constant. From our transport data, we estimated $l_T\approx600$ nm at $T=0.6$ K. As can be seen in Fig. 3, the available experimental data points roughly follow the trend of the calculated curve by using Eq. (2) and assuming $\beta=1$ and $l_\phi=430$ nm. The latter value is close to l_ϕ previously found for InN wires.[29] For the limit $l_\phi<L$, a correlation field according to $B_c=0.95\Phi_0/dl_\phi$ is expected.[21] As confirmed in Fig. 2(b), most experimental values of B_c are close to the calculated one.

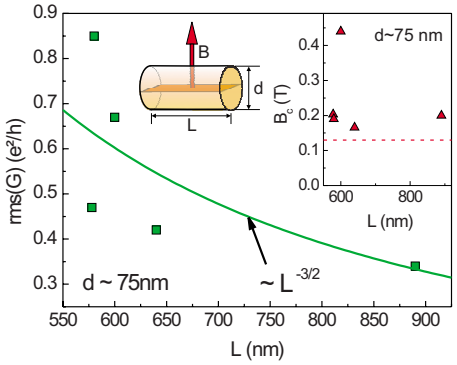

FIG. 3. (Color online) rms(G) for wires with a diameter of 75 ± 5 nm as a function of wire length L (squares). The magnetic field is oriented perpendicular to the wire axis. The calculated decrease of rms(G) proportional to $L^{-3/2}$ is plotted as a solid line. The inset shows B_c vs L for wires with $d\approx75$ nm. The dashed line corresponds to the calculated value of B_c assuming $l_\phi=430$ nm.

If one compares the rms(G) values for wires with $d\approx75$ nm and B axially oriented (not shown here) with the corresponding values for B perpendicularly oriented, one finds that both are in the same range. Thus, it can be concluded that the fluctuation amplitude does not significantly depend on the magnetic field orientation. This is in contrast to the correlation field, where one finds a systematic dependence on the orientation of B.

In order to discuss the latter aspect in more detail, the correlation field was studied for various tilt angles θ of the magnetic field. Figure 4 shows B_c of sample D if θ is increased from 0° to 90°. The inset of Fig. 4 illustrates how θ is defined. Obviously, B_c decreases with increasing tilt angle θ. As explained above, the value of B_c is a measure of the maximum area normal to B, which is enclosed phase coherently by the electron waves in the wire [see Fig. 4 (schematics)]. As long as $\theta\leq\arctan(L/d)$, this maximum area is given

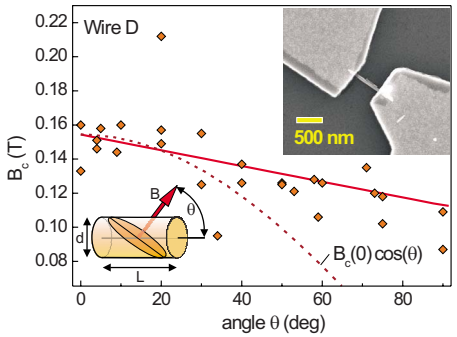

FIG. 4. (Color online) Correlation field B_c of wire D as a function of the angle θ between the wire axis and B. The solid line represents a linear fit. The broken line corresponds to the theoretically expected B_c if phase-coherent transport is assumed in the complete wire. The left-hand-side inset shows a schematics of the geometrical situation. The right-hand-side inset shows a micrograph of a 580-nm-long wire with a diameter of 66 nm.

by $A(\theta)=\pi d^2/4\cos\theta$. The expected θ dependence of the correlation field is then given by $B_c(\theta)=B_c(0)\cos(\theta)$, with $B_c(0)$ as the correlation field at $\theta=0$. As can be seen in Fig. 4, the calculated correlation field B_c, which corresponds to fully phase-coherent transport, decreases much faster with increasing θ than the experimentally determined values. The experimental situation is better described by a linear decrease. As was discussed before, for this particular wire, $A(0)$ is already larger than the maximum phase-coherent area. Thus, by changing the tilt angle, the effective area for phase coherence is only slightly changed. Furthermore, the orientation dependence of the parameter α might also account for the slow decrease of B_c with θ.

In conclusion, the conductance fluctuations of InN nanowires with various lengths and diameters were investigated. We found that for an axially oriented magnetic field, the correlation field B_c and thus the area where phase-coherent transport is maintained are limited by the wire cross section perpendicular to B. In contrast, rms(G) decreases with the wire length, since this quantity also depends on the propagation of the electron waves along the wire axis. If the magnetic field is perpendicularly oriented, we found that for long wires, B_c is limited by l_ϕ rather than by the length L. Our investigations demonstrate that phase-coherent transport can be maintained in InN nanowires, which is an important prerequisite for the design of quantum device structures based on this material system.

*th.schaepers@fz-juelich.de

[1] C. Thelander, P. Agarwal, S. Brongersma, J. Eymery, L. Feiner, A. Forchel, M. Scheffler, W. Riess, B. Ohlsson, U. Gösele, and L. Samuelson, Mater. Today **9**, 28 (2006).
[2] W. Lu and C. M. Lieber, J. Phys. D **39**, R387 (2006).
[3] K. Ikejiri, J. Noborisaka, S. Hara, J. Motohisa, and T. Fukui, J. Cryst. Growth **298**, 616 (2007).
[4] M. T. Björk, B. J. Ohlsson, C. Thelander, A. I. Persson, K. Deppert, L. R. Wallenberg, and L. Samuelson, Appl. Phys. Lett. **81**, 4458 (2002).
[5] T. Bryllert, L.-E. Wernersson, T. Lowgren, and L. Samuelson, Nanotechnology **17**, 227 (2006).
[6] Y. Li, J. Xiang, F. Qian, S. Gradecak, Y. Wu, H. Yan, D. Blom, and C. M. Lieber, Nano Lett. **6**, 1468 (2006).
[7] S. D. Franceschi, J. A. van Dam, E. P. A. M. Bakkers, L. Feiner, L. Gurevich, and L. P. Kouwenhoven, Appl. Phys. Lett. **83**, 344 (2003).
[8] C. Fasth, A. Fuhrer, M. T. Bjork, and L. Samuelson, Nano Lett. **5**, 1487 (2005).
[9] A. Pfund, I. Shorubalko, R. Leturcq, and K. Ensslin, Appl. Phys. Lett. **89**, 252106 (2006).
[10] A. Fuhrer, C. Fasth, and L. Samuelson, Appl. Phys. Lett. **91**, 052109 (2007).
[11] J. A. van Dam, Y. V. Nazarov, E. P. A. M. Bakkers, S. D. Franceschi, and L. P. Kouwenhoven, Nature (London) **442**, 667 (2006).
[12] C. H. Liang, L. C. Chen, J. S. Hwang, K. H. Chen, Y. T. Hung, and Y. F. Chen, Appl. Phys. Lett. **81**, 22 (2002).
[13] C.-Y. Chang, G.-C. Chi, W.-M. Wang, L.-C. Chen, K.-H. Chen, F. Ren, and S. J. Pearton, Appl. Phys. Lett. **87**, 093112 (2005).
[14] R. Calarco and M. Marso, Appl. Phys. A: Mater. Sci. Process. **87**, 499 (2007).
[15] C. W. J. Beenakker and H. van Houten, in *Solid State Physics*, edited by H. Ehrenreich and D. Turnbull (Academic, New York, 1991), Vol. 44, p. 1.
[16] J. J. Lin and J. P. Bird, J. Phys.: Condens. Matter **14**, R501 (2002).
[17] C. P. Umbach, S. Washburn, R. B. Laibowitz, and R. A. Webb, Phys. Rev. B **30**, 4048 (1984).
[18] A. D. Stone, Phys. Rev. Lett. **54**, 2692 (1985).
[19] P. A. Lee and A. D. Stone, Phys. Rev. Lett. **55**, 1622 (1985).
[20] B. Al'tshuler, Pis'ma Zh. Eksp. Teor. Fiz. **41**, 530 (1985) [JETP Lett. **41**, 648 (1985)].
[21] P. A. Lee, A. D. Stone, and H. Fukuyama, Phys. Rev. B **35**, 1039 (1987).
[22] T. J. Thornton, M. Pepper, H. Ahmed, G. J. Davies, and D. Andrews, Phys. Rev. B **36**, 4514 (1987).
[23] C. W. J. Beenakker and H. van Houten, Phys. Rev. B **37**, 6544 (1988).
[24] A. E. Hansen, M. T. Björk, I. C. Fasth, C. Thelander, and L. Samuelson, Phys. Rev. B **71**, 205328 (2005).
[25] T. Stoica, R. J. Meijers, R. Calarco, T. Richter, E. Sutter, and H. Lüth, Nano Lett. **6**, 1541 (2006).
[26] R. A. Jalabert, H. U. Baranger, and A. D. Stone, Phys. Rev. Lett. **65**, 2442 (1990).
[27] J. P. Bird, D. K. Ferry, R. Akis, Y. Ochiai, K. Ishsibashi, Y. Aoyagi, and T. Sugano, Europhys. Lett. **35**, 529 (1996).
[28] I. Mahboob, T. D. Veal, C. F. McConville, H. Lu, and W. J. Schaff, Phys. Rev. Lett. **92**, 036804 (2004).
[29] Ch. Blömers, Th. Schäpers, T. Richter, R. Calarco, H. Lüth, and M. Marso, Appl. Phys. Lett. **92**, 132101 (2008).